Magic wavelengths in the alkaline earth ions

Jasmeet Kaur[a], Sukhjit Singh[a], Bindiya Arora[a*] and B. K. Sahoo [b†]

[a]*Department of Physics, Guru Nanak Dev University, Amritsar, Punjab-143005, India and*
[b]*Theoretical Physics Division, Physical Research Laboratory, Navrangpura, Ahmedabad-380009, India*
(Dated: Received date; Accepted date)

We present magic wavelengths for the nS - $nP_{1/2,3/2}$ and nS - $mD_{3/2,5/2}$ transitions, with the respective ground and first excited D states principal quantum numbers n and m, in the Mg$^+$, Ca$^+$, Sr$^+$ and Ba$^+$ alkaline earth ions for linearly polarized lights by plotting dynamic polarizatbilities of the nS, $nP_{1/2,3/2}$ and $mD_{3/2,5/2}$ states of the ions. These dynamic polarizabilities are evaluated by employing a relativistic all-order perturbative method and their accuracies are ratified by comparing their static values with the available high precision experimental or other theoretical results. Moreover, some of the magic wavelengths identified by us in Ca$^+$ concurs with the recent measurements reported in [**Phys. Rev. Lett. 114, 223001 (2015)**]. Knowledge of these magic wavelengths are propitious to carry out many proposed high precision measurements trapping the above ions in the electric fields with the corresponding frequencies.

State-insensitive trapping techniques have lead to tremendous advancements in the manipulation and control of atoms in far detuned optical traps. In this approach, the atoms are trapped at the wavelengths (related to frequencies) of an external electric field at which the differential light shift of an atomic transition, that is intended to be probed, due to the Stark effects nullify. These wavelengths are specially referred to as magic wavelengths (λ_{magic}s)[1]. It has been demonstrated earlier ability of trapping neutral atoms inside high-Q cavities at λ_{magic}s in the strong coupling regime, which is important in the quantum computation and communication schemes [2]. This technique is now widely used to carry out many high precision measurements by eliminating large systematics due to stray electric fields. Another notable application of these wavelengths is to perform clock frequency measurements [3], especially for optical frequency standards [4], that are in turn useful to probe temporal and spatial variations of the fundamental constants [5] and improving global positioning systems [6]. Knowing λ_{magic}s of atomic systems are also very useful in the field of quantum state engineering [7], extracting out precise values of the oscillator strengths [8], etc. because of which extensive studies, both experimentally and theoretically, have been carried out in many atoms recently [6, 9–12]. On the other hand, singly charged alkaline earth ions are advantageous to carry out very high precision measurements using ion trapping and laser cooling techniques. Some of the prominent examples are the optical frequency standards [13, 14], probing variation of fundamental constants [3, 5], parity non-conservation effects [15, 16] etc. Advantages of these ions owe to their metastable D states that provide longer probe times during interrogation of measurements. To reduce system-

atics in these measurements, state insensitive measurements can be more pertinent that will require knowledge of λ_{magic}s in these ions. In fact, λ_{magic}s for the $4S \rightarrow 3D_{3/2,5/2}$ and $4S \rightarrow 4P_{1/2,3/2}$ transitions in Ca$^+$ are recently observed [17].

In this Rapid Communication, we report λ_{magic}s for the $nS - nP_{1/2,3/2}$ and $nS - mD_{3/2,5/2}$ transitions in the Mg$^+$, Ca$^+$, Sr$^+$ and Ba$^+$ ions, for the principal quantum numbers of the ground state n and of the first excited D states m of the respective ions, for the commonly used linearly polarized lights in the experiments by evaluating dynamic dipole polarizabilities of these ions accurately.

Dominant contribution to the change in energy of a state $|j_n, m_n\rangle$ with angular momentum j_n and its component m_n of an atomic system due to interaction with an external electric field $\mathcal{E}(\omega)$ of frequency ω is given by

$$\triangle E_{Stark} \approx -\frac{1}{2}\alpha_n(\omega)\mathcal{E}^2(\omega), \qquad (1)$$

where $\alpha_n(\omega)$ is the dynamic dipole polarizability of the atomic state $|j_n, m_n\rangle$ and given by

$$\alpha_n(\omega) = \alpha_n^{(0)}(\omega) + \frac{3m_j^2 - j_n(j_n + 1)}{j_n(2j_n - 1)}\alpha_n^{(2)}(\omega), \quad (2)$$

for the scalar and tensor components as $\alpha_n^{(0)}(\omega)$ and $\alpha_n^{(2)}(\omega)$, respectively. Expressions for these quantities in terms of the reduced electric dipole (E1) matrix elements can be found in Refs. [9–11]. As discussed in our previous work [18], we estimate $\alpha_n^{(k)}$s (for $k = 0, 2$) by expressing

$$\alpha_n^{(k)} = \alpha_n^{(k)}(c) + \alpha_n^{(k)}(vc) + \alpha_n^{(k)}(v) \qquad (3)$$

with the notations c, vc and v representing the contributions due to the core, core-valence and valence correlation effects, respectively. Dominant valence correlations are estimated by calculating electric dipole (E1) matrix elements between many low-lying intermediate states and referred to as "Main" result. This is evaluated using
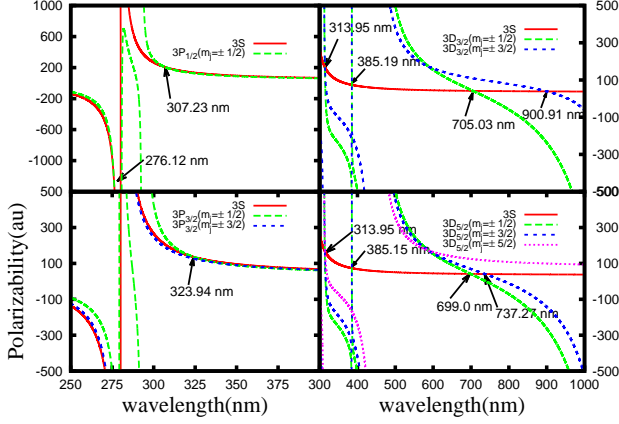
FIG. 1: (Color online) Dynamic polarizabilities (in au) of the $3S_{1/2}$, $3P_{1/2,3/2}$ and $3D_{3/2,5/2}$ states in Mg$^+$. Arrows indicate positions of magic wavelengths (λ_{magic}s) in nm.

an all order relativistic coupled-cluster method with the singles and doubles approximation (SD method) as described in [19, 20]. Other small contributions from the higher excited states (referred to as "Tail" contribution), core and core-valence correlations are estimated using lower order perturbative methods as described in [18]. To construct the single particle orbitals for the SD method, we have used total 70 B-spline functions with a cavity of radius $R = 220$ au. However, a few E1 matrix elements involving the $F_{5/2,7/2}$ states in Ba$^+$ are taken from [21] to use as many as E1 matrix elements for more accurate evaluations of the Main contributions to α_ns of the $5D$ states of this ion. Estimated static polarizabilities in the above procedure of the considered ground and excited states of the alkaline earth metal ions using these matrix elements and experimental energies from national institute of standards and technology (NIST) [22] are listed in the Supplemental material along with the individual core, core-valence and Tail contributions. These values are also compared with the available precise experimental results and theoretical calculations. We find excellent agreement between our results with these values implying that our calculations are precise enough to predict the magic wavelengths in the considered ions reliably.

In Tables I, II, III and IV, we list λ_{magic}s for the $nS - nP_{1/2,3/2}$ and $nS - mD_{3/2,5/2}$ transitions in the Mg$^+$, Ca$^+$, Sr$^+$ and Ba$^+$ ions respectively. They are obtained by locating the crossings between the dynamic polarizabilities of the nS, $nP_{1/2}$, $nP_{3/2}$, $mD_{3/2}$, and $mD_{5/2}$ states of Mg$^+$,Ca$^+$, Sr$^+$ and Ba$^+$ plotted against the frequencies as shown in Figs. 1, 2, 3 and 4 respectively. The arrows in the figures indicate the positions of $\lambda_{\mathrm{magic}}(\mathrm{avg})$ values which are the average of the magic wavelengths at different m_j sub-levels. The $\lambda_{\mathrm{magic}}(\mathrm{avg})$ are not presented for cases where magic wavelengths are (a) not identified for all m_j sub-levels, (b) supporting different kind of trapps for all m_j sublevels (c) separated by large

TABLE I: Magic wavelengths (λ_{magic}s) in nm and corresponding polarizabilities (in au) in the Mg$^+$ ion. List of the resonant wavelengths (λ_{res}s) and λ_{magic}s are also given sequentially in increasing order to indicate their respective placements.

| Resonance Transition	λ_{res}	$|m_j|$	λ_{magic}	$\alpha(\lambda_{\mathrm{magic}})$
		$3S - 3P_{1/2}$		
$3P_{1/2}$-$3D_{3/2}$	279.0777	1/2	276.12	−1267.54
$3P_{1/2}$-$3S_{1/2}$	280.2704			
$3P_{1/2}$-$4S_{1/2}$	292.8683	1/2	307.23	202.59
Transition		$3S - 3P_{3/2}$		
$3P_{3/2} - 3D_{3/2}$	279.7930			
$3P_{3/2} - 3D_{5/2}$	279.7998			
$3P_{3/2} - 3S_{1/2}$	279.5528			
$3P_{3/2} - 4S_{1/2}$	293.6510	1/2	323.94	136.51
Transition		$3S - 3D_{3/2}$		
$3D_{3/2} - 5F_{5/2}$	310.4809	1/2	313.73	169.42
		3/2	314.18	167.53
$3D_{3/2} - 5P_{3/2}$	384.8335	3/2	385.01	72.56
$3D_{3/2} - 5P_{1/2}$	385.0385	1/2	385.38	73.47
$3D_{3/2} - 4F_{5/2}$	448.1327	1/2	705.03	41.44
		3/2	900.91	38.67
$3D_{3/2} - 4P_{3/2}$	1091.5270			
$3D_{3/2} - 4P_{1/2}$	1095.1779			
Transition		$3S - 3D_{5/2}$		
$3D_{5/2} - 5F_{7/2}$	310.4715			
$3D_{5/2} - 5F_{5/2}$	310.4721	1/2	313.67	169.66
		3/2	313.80	169.01
		5/2	314.39	166.70
$3D_{5/2} - 5P_{3/2}$	384.8209	3/2	385.12	73.58
		1/2	385.17	73.56
$3D_{5/2} - 4F_{7/2}$	448.1130			
$3D_{5/2} - 4F_{5/2}$	448.1150	1/2	699.0	41.57
		3/2	737.27	40.79
$3D_{5/2} - 4P_{3/2}$	1091.423			
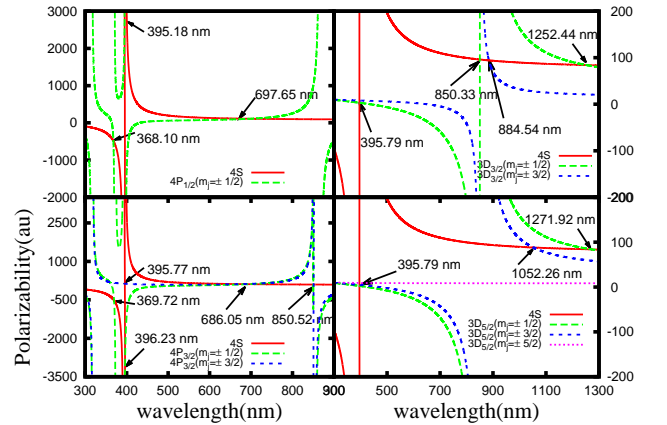
FIG. 2: (Color online) Dynamic polarizabilities (in au) of the $4S_{1/2}$, $4P_{1/2,3/2}$ and $3D_{3/2,5/2}$ states in Ca$^+$. Locations of average λ_{magic}s (in nm) are indicated by arrows.

wavelengths for different m_j sub-levels. We also give the total α_n values at the corresponding λ_{magic}s considering different m_j values in the tables. Before we proceed in

TABLE II: λ_{magic}s (in nm) and corresponding polarizabilities (in au) in the Ca$^+$ ion. λ_{res} are also presented to identify the placements of λ_{magic}s clearly between two resonant wavelengths. Results from this work ([T]) are compared with the findings from Ref. [8].

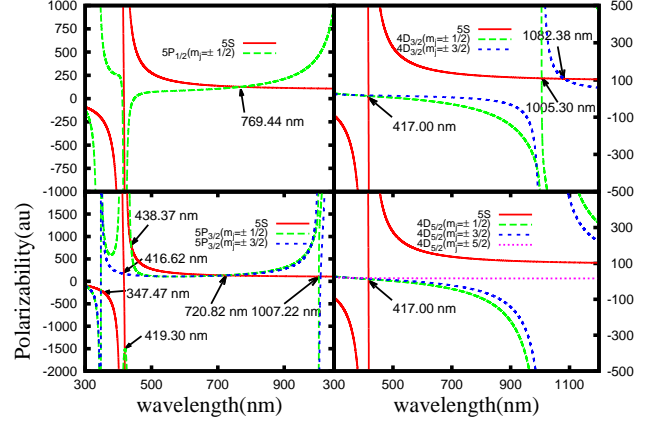| Resonances	λ_{res}	$|m_j|$	λ_{magic}	$\alpha(\lambda_{\mathrm{magic}})$	Reference
Transition			$4S - 4P_{1/2}$		
$4P_{1/2} - 4D_{3/2}$	315.887	1/2	368.10	−485.18	[T]
			368.0149	−477.2554	[8]
$4P_{1/2} - 5S_{1/2}$	370.603	1/2	395.18	2933.47	[T]
			395.1807	2896.7954	[8]
$4P_{1/2} - 4S_{1/2}$	396.847	1/2	697.65	110.39	[T]
			690.817	110.0849	[8]
$4P_{1/2} - 3D_{3/2}$	866.214				
Transition			$4S - 4P_{3/2}$		
$4P_{3/2} - 4D_{5/2}$	317.933				
$4P_{3/2} - 4D_{3/2}$	318.128	1/2	369.72	−520.85	[T]
			369.6393	−512.1655	[8]
$4P_{3/2} - 5S_{1/2}$	373.690				
$4P_{3/2} - 4S_{1/2}$	393.366	3/2	395.77	125.27	[T]
			395.774	123.4906	[8]
		1/2	396.23	−3118.47	[T]
			396.2315	−3077.3881	[8]
$4S_{1/2} - 4P_{1/2}$	396.847	3/2	678.35	113.38	[T]
			672.508	113.0150	[8]
		1/2	693.76	110.96	[T]
			687.022	110.6606	[8]
$4P_{3/2} - 3D_{3/2}$	849.802	1/2	850.12	81.57	[T]
		3/2	850.92	96.09	[T]
$4P_{3/2} - 3D_{5/2}$	854.209				
Transition			$4S - 3D_{3/2}$		
$4S_{1/2} - 4P_{3/2}$	393.366	1/2	395.80	3.13	[T]
			395.7981	1.1711	[8]
		3/2	395.79	8.02	[T]
			395.7970	7.1019	[8]
$4S_{1/2} - 4P_{1/2}$	396.847				
$3D_{3/2} - 4P_{3/2}$	849.802	1/2	850.33	96.12	[T]
			850.335	95.0011	[8]
$3D_{3/2} - 4P_{1/2}$	866.214	3/2	884.54	94.23	[T]
			887.382	92.9908	[8]
		1/2	1252.44	84.17	[T]
			1308.590	82.4644	[8]
Transition			$4S - 3D_{5/2}$		
$4S_{1/2} - 4P_{3/2}$	393.366	1/2	395.79	2.44	[T]
			395.7982	0.5371	[8]
		3/2	395.79	3.49	[T]
			395.7978	3.1792	[8]
		5/2	395.79	8.83	[T]
			395.7968	8.4633	[8]
$4S_{1/2} - 4P_{1/2}$	396.847				
$3D_{5/2} - 4P_{3/2}$	854.209	3/2	1052.26	88.06	[T]
			1074.336	86.4837	[8]
		1/2	1271.92	83.90	[T]
			1338.474	82.1167	[8]

FIG. 3: (Color online) Dynamic polarizabilities (in au) of the $5S_{1/2}$, $5P_{1/2,3/2}$ and $4D_{3/2,5/2}$ states in Sr$^+$. Arrows indicate positions of the average λ_{magic} in nm.

considered in this work. Therefore, α_ns of the nS states are generally small except in the close vicinity of these transitions. In contrast, α_ns of the nP and mD states can have significant contributions from several resonant transitions in the considered wavelength range. Thus, they are expected to cross with α_ns of the nS states in between these resonant transitions. We also list the resonant wavelengths (λ_{res}) in the above tables to highlight respective placements of λ_{magic}s. We find similar trends in locating magic wavelengths for all the considered ions, except for few cases where λ_{magic}s are missing.

Mg$^+$: We are able to locate two λ_{magic}s magic wavelengths for the $3S - 3P_{1/2}$ transition in Mg$^+$, one just before the $3P_{1/2} - 3D$ resonant transition at 276.12 nm and one just after the $3P_{1/2} - 4S$ resonant transition at 307.23 nm. The first λ_{magic} supports a blue detuned trap, whereas the second one a red detuned trap. However, only one λ_{magic} for the $3S - 3P_{3/2}(m_j = \pm 1/2)$ transition is located at 323.94 nm and nothing is found for the $3S - 3P_{3/2}(m_j = \pm 3/2)$ transition. On the other hand, three λ_{magic}s are identified for the $3D_{3/2} - 3S$ transition placed between six different resonances. First one is located around 314 nm between the $3D_{3/2} - 5F_{5/2}$ and $3D_{3/2} - 5P_{3/2}$ resonant transitions. The next λ_{magic} is located at the sharp intersection of polarizability curves close to the $3D_{3/2} - 5P_{3/2}$ and the $3D_{3/2} - 5P_{1/2}$ resonances as seen in Fig. 1. The last λ_{magic} is located at 705.03 nm for $m_j = \pm 1/2$ and 900.91 nm for $m_j = \pm 3/2$ sub-levels, hence it is of limited experimental use. For the $3S - 3D_{5/2}$ transition, only one λ_{magic} appears for all m_j sub-levels around 314 nm. All the observed λ_{magic}s along with the λ_{res}s are tabulated in Table I. It can be noticed from this table that most of these magic wavelengths favor weak red detuned traps.

Ca$^+$: At least three λ_{magic}s are located for the $4P_{1/2} - 4S$ transition in Ca$^+$ at 368.10, 395.18 and 697.65 nms between the $4P_{1/2} - 4D_{3/2}$, $4P_{1/2} - 5S$, $4P_{1/2} - 4S$ and

presenting λ_{magic}s, we would like to clarify that α_ns of the nS states can have two important resonant transitions ($nS - nP_{1/2}$ and $nS - nP_{3/2}$) in the wavelength range

TABLE III: λ_{magic}s (in nm) and their corresponding polarizabilities (in au) in Sr$^+$ and λ_{res} contributing to the polarizabilities of the transitional states are also listed.

Resonances	λ_{res}	$|m_j|$	λ_{magic}	$\alpha(\lambda_{\mathrm{magic}})$
Transition			$5S - 5P_{1/2}$	
$5P_{1/2} - 5D_{3/2}$	338.0711			
$5P_{1/2} - 6S_{1/2}$	416.1796			
$5P_{1/2} - 5S_{1/2}$	421.5524	1/2	769.44	126.34
$5P_{1/2} - 4D_{3/2}$	1091.4874			
Transition			$5S - 5P_{3/2}$	
$5P_{3/2} - 5D_{5/2}$	346.4457	3/2	347.38	−204.86
$5P_{3/2} - 5D_{3/2}$	347.4887	1/2	347.57	−205.66
$5P_{3/2} - 5S_{1/2}$	407.7714	3/2	416.62	168.54
		1/2	419.30	−1521.68
$5S_{1/2} - 5P_{1/2}$	421.5524			
$5P_{3/2} - 6S_{1/2}$	430.5447	1/2	438.37	817.75
		1/2	716.72	134.25
		3/2	724.92	132.83
$5P_{3/2} - 4D_{3/2}$	1003.6654	1/2	1004.47	108.08
		3/2	1009.80	108.90
$5P_{3/2} - 4D_{5/2}$	1032.7309			
Transition			$5S - 4D_{3/2}$	
$5S_{1/2} - 5P_{3/2}$	407.7714	3/2	417.00	17.36
		1/2	417.00	13.83
$5S_{1/2} - 5P_{1/2}$	421.5524			
$4D_{3/2} - 5P_{3/2}$	1003.6654	1/2	1005.30	108.93
		3/2	1082.38	106.29
$4D_{3/2} - 5P_{1/2}$	1091.4874			
Transition			$5S - 4D_{5/2}$	
$5S_{1/2} - 5P_{3/2}$	407.7714	1/2	417.01	12.16
		5/2	417.00	18.43
		3/2	417.00	14.25
$5S_{1/2} - 5P_{1/2}$	421.5524			
$4D_{5/2} - 5P_{3/2}$	1032.7309			

TABLE IV: λ_{magic}s (in nm) and their corresponding polarizabilities (in au) in Ba$^+$. λ_{res}s are also given to identify the placements of λ_{magic}s between them.

| Resonances	λ_{res}	$|m_j|$	λ_{magic}	$\alpha(\lambda_{\mathrm{magic}})$
Transition			$6S - 6P_{1/2}$	
$6P_{1/2} - 8S_{1/2}$	264.72608	1/2	323.33	−93.74
$6P_{1/2} - 6D_{3/2}$	389.17790	1/2	451.73	−4574.49
$6P_{1/2} - 7S_{1/2}$	452.4926	1/2	468.90	953.80
$6P_{1/2} - 6S_{1/2}$	493.4077	1/2	599.28	311.58
$6P_{1/2} - 5D_{3/2}$	649.6898			
Transition			$6S - 6P_{3/2}$	
$6P_{3/2} - 8S_{1/2}$	277.13528	3/2	348.85	−133.47
		1/2	360.63	−158.70
$6P_{3/2} - 6D_{5/2}$	413.06491			
$6P_{3/2} - 6D_{3/2}$	416.60014	1/2	416.66	−460.38
		3/2	416.06	−459.32
$6P_{3/2} - 6S_{1/2}$	455.4033	3/2	475.72	374.67
$6P_{3/2} - 7S_{1/2}$	489.9927	1/2	552.60	441.01
		3/2	561.01	406.42
$6S_{1/2} - 6P_{1/2}$	493.4077			
$6P_{3/2} - 5D_{3/2}$	585.3675	1/2	586.24	336.10
		3/2	593.40	321.95
$6P_{3/2} - 5D_{5/2}$	614.1713			
Transition			$6S - 5D_{3/2}$	
$6S_{1/2} - 6P_{3/2}$	455.4033	3/2	480.44	15.88
		1/2	480.81	−15.82
$6S_{1/2} - 6P_{1/2}$	493.4077			
$5D_{3/2} - 6P_{3/2}$	585.3675	1/2	585.98	336.18
		3/2	592.46	323.72
$5D_{3/2} - 6P_{1/2}$	649.6898	1/2	767.81	194.05
Transition			$6S - 5D_{5/2}$	
$6S_{1/2} - 6P_{3/2}$	455.4033	5/2	480.26	31.04
		3/2	480.71	−7.19
		1/2	480.93	−26.46
$6S_{1/2} - 6P_{1/2}$	493.4077			
$5D_{5/2} - 6P_{3/2}$	614.1713	3/2	666.64	239.13
		1/2	718.18	211.13
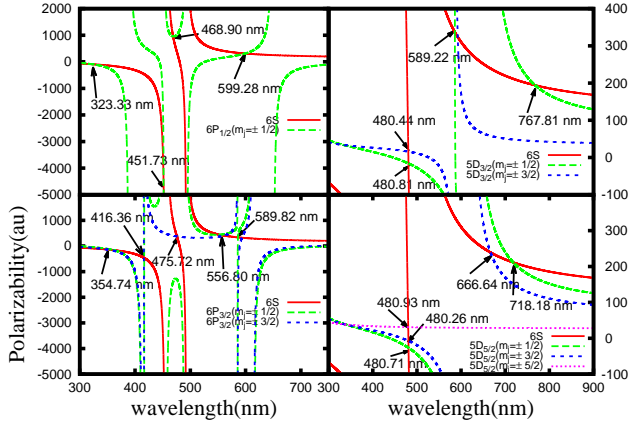
FIG. 4: (Color online) Dynamic polarizabilities (in au) of the $6S_{1/2}$, $6P_{1/2,3/2}$ and $5D_{3/2,5/2}$ states in Ba$^+$ with their average λ_{magic}s (in nm) pointed by arrows.

$4P_{1/2} - 3D_{3/2}$ resonant transitions. A good agreement is found between our results and findings by Tang et. al. [8] except for our λ_{magic} at 697.65 nm, which is red

detuned as compared to their value. Similarly, a total of four λ_{magic}s are located for the $4S - 4P_{3/2}$ transition as shown in Fig. 2 and listed in Table II. We also find λ_{magic}s at 395.77 nm and 396.23 nm for the $4S - 4P_{3/2}$ transition within the fine structure splittings of the $4P$ states which coincides with the experimental observations at 395.7992(7) nm and 395.7990(7) nm respectively [17]. Similar to the $4P_{1/2} - 4S$ transition, the other observed λ_{magic}s at 678.35 nm and 693.76 nm are red detuned as compared to findings in Ref. [8]. Moreover, they have missed a λ_{magic} around 850 nm which lies in between the $4P_{3/2} - 3D_{3/2}$ and $4P_{3/2} - 3D_{5/2}$ resonant transitions. λ_{magic}s for the $4S - 3D_{3/2}$ and $4S - 3D_{5/2}$ transitions, detected between the fine structure splitting of the $4P$ state at 395.79 nm, offer a scope to trap Ca$^+$ at very small polarizabilities and are not much of practical use. As seen in Fig. 2, α_ns of the $3D_{5/2}(m_j = \pm 5/2)$ state attain a constant value through out the wavelength range considered in this work. Consequently, only one crossing is noticed for this state at 395 nm when α_n of the $4S$ state changes

sign close to the $4S - 4P$ resonances. The other identified λ_{magic}s at 1052.26, 1252.44 and 1271.92 nms for the $4S-3D_{3/2}$ and $4S-3D_{5/2}$ transitions with different m_j values are blue detuned compared to the earlier findings of Ref. [8]. The possible reasons for these disagreements could be that the plots for α_ns of the transitional states cross at very small angles at these wavelengths thus making them very in-distinctive. Moreover, Tang *et. al.* have performed semi-empirical calculations of polarizabilities in the relativistic framework that do not take into account electron correlation effects rigorously like our SD method.

Sr$^+$: From Fig. 3, we are able to locate only one magic wavelength at 769.44 nm for the $5S$ - $5P_{1/2}$ transition of Sr$^+$. As given in Table III, λ_{magic}s for the $5S-5P_{3/2}$ transition are, however, systematically placed between various resonances. We also locate a crossing between the $5S$ and $5P_{3/2}(m_j = \pm 1/2)$ states at 438.37 nm. All identified λ_{magic}s for the $5S - 5P_{3/2}$ transition are typically small in magnitude with exception for $\lambda_{\mathrm{magic}} = 419.302$ nm. At this λ_{magic}, it is recommended to use blue tuned trap for the $m_j = \pm 1/2$ sub-levels of Sr$^+$. For the $4D_{3/2} \to 5S$ transition, $\lambda_{\mathrm{magic}} = 1007.22$ nm lies in the infrared region and is recommended for red detuned trap. In Fig. 3, we also observe that α_ns for the transitional states at $\lambda_{\mathrm{magic}} = 417$ nm for the $5S-4D_{3/2}$ and $5S - 4D_{5/2}$ transitions are very small (almost approach to zero). Therefore, it may not be advantageous to trap the Sr$^+$ ion at this wavelength.

Ba$^+$: Four λ_{magic}s are found for the $6S - 6P_{1/2}$ transition in Ba$^+$ at 323.33, 451.73, 468.90 and 599.28 nms among which $\lambda_{\mathrm{magic}} = 451.73$ nm is in direct vicinity of the $6P_{1/2} - 7S_{1/2}$ resonance (within 0.8 nm) yielding a very large negative value of α_n. However, the other λ_{magic}s are at far distances from the photon excitation energies of the resonant transitions yielding small α_ns. We also identify at least five λ_{magic}s for the $6P_{3/2}$-$6S_{1/2}$ transition placed systematically between various resonant transitions. Similarly, several λ_{magic}s are also located for the $6S$-$5D_{3/2}$ and $6S$-$5D_{5/2}$ transitions as seen in Fig. 4 in the wavelength range 300-800 nm and listed in Table IV.

Conclusion: By determining dynamic dipole polarizabilities of the ground nS and the first excited $nP_{1/2,3/2}$ and $mD_{3/2,5/2}$ states, many magic wavelengths of the $nS-nP_{1/2,3/2}$ and $nS-mD_{3/2,5/2}$ transitions of the Mg$^+$, Ca$^+$, Sr$^+$ and Ba$^+$ alkaline earth metal ions are identified. Occurrence of magic wavelengths are predicted between the resonant wavelengths which will be very helpful to perform high precision measurements in the above ions using both the red and blue tuned trapping techniques.

[1] H. Katori, T. Ido, and M. K. Gonokami, J. Phys. Soc. Jpn. **68**, 2479 (1999).
[2] J. McKeever, J. R. Buck, A. D. Boozer, A. Kuzmich, H.-C. Nagerl, D. M. Stamper-Kurn, and H. J. Kimble, Phys. Rev. Lett. **90**, 133602 (2003).
[3] H. S. Margolis, J. Phys. B **42**, 154017 (2009).
[4] V. D. Ovsiannikov and V. G. Palchikov, Laser Physics **15**, 1040 (2005).
[5] S. G. Karshenboim and E. Peik, *Astrophysics, Clocks and Fundamental Constants*, 3-540-21967-6 (Springer, Springer Verlag Berlin Heidelberg, 2004).
[6] T. Hong, C. Cramer, E. Cook, W. Nagourney, and E. N. Fortson, Opt. Lett. **30**, 2644 (2005).
[7] C. A. Sackett, D. Kielpinski, B. E. King, C. Langer, V. Meyer, C. J. Myatt, M. Rowe, Q. A. Turchette, W. M. Itano, D. J. Wineland, et al., Nature **404**, 256 (2000).
[8] Y. B. Tang, H. X. Qaio, T. Y. Shi, and J. Mitroy, Phys. Rev. A **87**, 042517 (2013).
[9] B. Arora, M. S. Safronova, and C. W. Clark, Phys. Rev A **76**, 052509 (2007).
[10] B. Arora and B. K. Sahoo, Phys. Rev. A **86**, 033416 (2012).
[11] B. K. Sahoo and B. Arora, Phys. Rev. A **87**, 023402 (2013).
[12] M. Takamoto, F.-L. Hong, R. Higashi, and H. Katori, Nature (London) **435**, 321 (2005).
[13] M. Kajita, Y. Li, K. Matsubara, K. Hayasaka, and M. Hosokawa, Phys. Rev. A **72**, 043404 (2005).
[14] P. Dubé, A. A. Madej, J. Bernard, L. Marmet, J. S. Boulanger, and S. Cundy, Appl. Phys. Lett. **95**, 033001 (2005).
[15] N. Fortson, Phys. Rev. Lett. **70**, 2383 (1993).
[16] B. K. Sahoo, P. Mandal, and M. Mukherjee, Phys. Rev. A **83**, 030502(R) (2011).
[17] P. Liu, Y. Huang, W. Bian, H. Shao, H. Guan, Y. Tang, C. Li, J. Mitroy, and K. Gao, Phys. Rev. Lett. **114**, 223001 (2015).
[18] J. Kaur, D. K. Nandy, B.Arora, and B. Sahoo, Phys. Rev A **91**, 012705 (2015).
[19] S. A. Blundell, W. R. Johnson, and J. Sapirstein, Phys. Rev A **43**, 3407 (1991).
[20] M. S. Safronova, A. Derevianko, and W. R. Johnson, Phys. Rev A **58**, 1016 (1998).
[21] B. K. Sahoo, L. W. Wansbeek, K. Jungmann, and R. G. E. Timmermans, Phys. Rev A **79**, 052512 (2009).
[22] A. Kramida, Y. Ralchenko, J. Reader, and N. A. T. (2012), *Nist atomic spectra database* (2012), (version 5). [Online]. Available: http://physics.nist.gov/asd [2012, December 12]. National Institute of Standards and Technology, Gaithersburg, MD.

Supplemental Material

In a sum-over-states approach the valence correlation contributions can be estimated using the expression

$$\alpha_n^{(0)}(v) \;=\; -\frac{2}{3(2j_n+1)} \sum_{p\neq n} \frac{(E_p-E_n)|\langle j_n||D||j_p\rangle|^2}{(E_n-E_p)^2-\omega^2} \quad (1)$$

and

$$\alpha_n^{(2)}(v) \;=\; -8\sum_{p\neq n}(-1)^{j_n+j_p+1} \left\{ \begin{array}{ccc} j_n & 1 & j_n \\ 1 & j_p & 2 \end{array} \right\}$$
$$\times \sqrt{\frac{5j_n(2j_n-1)}{6(j_n+1)(2j_n+1)(2j_n+3)}}$$
$$\times \frac{(E_p-E_n)|\langle j_n||D||j_p\rangle|^2}{(E_n-E_p)^2-\omega^2}, \quad (2)$$

where p stands for the excited intermediate states, js are angular momentum of the correspond state, Es are their energies and D is the dipole operator. It is required to calculate a sufficient number of atomic states so that as many as E1 matrix elements $\langle j_n||D||j_p\rangle$ can be evaluated to estimate contributions to the $\alpha_n^{(k)}$ values. Contributions from the higher excited states, especially from the continuum, are usually small and they can be estimated using a lower order many-body method to a reasonable accuracy as suggested in our previous work [1]. We refer the above described dominant contribution as "Main" and the later contribution as "Tail" to $\alpha_n^{(k)}(v)$.

Similarly, the core-valence contribution can be estimated by expressing as

$$\alpha_n^{(0)}(cv) \;=\; -\frac{2}{3(2j_n+1)} \sum_{c} \frac{(E_c-E_n)|\langle j_n||D||j_c\rangle|^2}{(E_n-E_c)^2-\omega^2} \quad (3)$$

and

$$\alpha_n^{(2)}(cv) \;=\; -8\sum_{c}(-1)^{j_n+j_c+1} \left\{ \begin{array}{ccc} j_n & 1 & j_n \\ 1 & j_c & 2 \end{array} \right\}$$
$$\times \sqrt{\frac{5j_n(2j_n-1)}{6(j_n+1)(2j_n+1)(2j_n+3)}}$$
$$\times \frac{(E_c-E_n)|\langle j_n||D||j_c\rangle|^2}{(E_n-E_c)^2-\omega^2}, \quad (4)$$

where c stands for core orbitals. This basically subtracts the extra contributions accounted by allowing the Pauli's exclusion principle of the valence electron in the determination of the atomic states. Typically, these contributions are extremely small in magnitude and can be estimated using a lower order many-body theory as in Ref. [1].

Expressions for the core contributions is given by

$$\alpha_n^{(0)}(c) \;=\; -\frac{2}{3} \sum_{c,p} \frac{(E_c-E_p)|\langle j_p||D||j_c\rangle|^2}{(E_p-E_c)^2-\omega^2}. \quad (5)$$

and

$$\alpha_n^{(2)}(c) \;=\; -8\sum_{c,p}(-1)^{j_p+j_c+1} \left\{ \begin{array}{ccc} j_p & 1 & j_p \\ 1 & j_c & 2 \end{array} \right\}$$
$$\times \sqrt{\frac{5j_n(2j_n-1)(2j_n+1)}{6(j_n+1)(2j_n+3)}}$$
$$\times \frac{(E_c-E_p)|\langle j_p||D||j_c\rangle|^2}{(E_p-E_c)^2-\omega^2}, \quad (6)$$

where c and p represent sums over core and virtual orbitals, respectively. It can be noticed that there appears an extra phase factor in the expression for the tensor polarizability. Since c and p sums over a complete set of c and p orbitals of a closed-core, therefore core contribution to the tensor polarizability nullifies. Again, the core contributions to the scalar polarizabilities for the states having common core are same since its expression is independent of j_n.

The first four low-lying allowed transitions are included in the evaluations of the "Main" contributions in the Mg$^+$, Ca$^+$ and Sr$^+$ ions, whereas only the first three low-lying allowed transitions are included in the Ba$^+$ ion. However, th efirst six low-lying E1 matrix elements are included in the estimation of "Main" contributions in the $3D_{3/2,5/2}$ states of the Ca$^+$ ion. These states are evaluated using a linearized version of the relativistic coupled-cluster method with the singles and doubles approximation (SD method) as described in Refs. [2, 3]. Atomic wave function of the $|j_n, m_n\rangle$ state in this method is given by

$$|\Psi_n\rangle \;=\; \left[1 + \sum_{pa}\rho_{pa}a_p^\dagger a_a + \frac{1}{2}\sum_{pqab}\rho_{pqab}a_p^\dagger a_q^\dagger a_b a_a \right.$$
$$\left. + \sum_{p\neq n}\rho_{pn}a_p^\dagger a_n + \sum_{pqa}a_p^\dagger a_q^\dagger a_a a_n \right] |\Phi_n\rangle, \quad (7)$$

where $|\Phi_n\rangle$ is considered to be the Dirac-Fock (DF) wave function constructed by

$$|\Phi_n\rangle = a_n^\dagger|\Phi_0\rangle \quad (8)$$

for the DF wave function $|\Phi_0\rangle$ of the closed-core. In the above expression, $a_i^\dagger$ and a_i represent for the creation and annihilation operators. The indices p, q represent for the virtual orbitals and the indices a, b refer to the occupied orbitals. ρs are the amplitudes of the excitations with the subscripts for the corresponding orbitals. The matrix element of D between states $|j_v m_v\rangle$ and $j_w m_w\rangle$ states is evaluated in this method by [4].

$$D_{vw} = \frac{\langle \psi_v|D|\Psi_w\rangle}{\sqrt{\langle \psi_v|\psi_v\rangle\langle \psi_w|\psi_w\rangle}}. \quad (9)$$

Combining E1 matrix elements obtained using the SD method with the experimental energies from the national

TABLE I: Calculated values of the static dipole polarizabilities of Ca$^+$, Sr$^+$, Ba$^+$ and Ra$^+$ alkaline earth metal ions. These values are compared with the other available theoretical and experimental results. References are given in the square brackets. The first four low-lying allowed transitions were included in the evaluations of the "Main" contributions in the Mg$^+$, Ca$^+$ and Sr$^+$ ions, whereas only the first three low-lying allowed transitions were included in the Ba$^+$ ion. In an exception, the first six low-lying E1 matrix elements were included in the estimation of "Main" contributions in the $3D_{3/2,5/2}$ states of the Ca$^+$ ion.

Mg$^+$	$\alpha^{(0)}(3S_{1/2})$	$\alpha^{(0)}(3P_{1/2})$	$\alpha^{(0)}(3P_{3/2})$	$\alpha^{(2)}(3P_{3/2})$	$\alpha^{(0)}(3D_{3/2})$	$\alpha^{(2)}(3D_{3/2})$	$\alpha^{(0)}(3D_{5/2})$	$\alpha^{(2)}(3D_{5/2})$
Main	34.50	30.89	31.18	1.32	185.35	-78.41	184.71	-111.13
Core	0.48	0.48	0.48	-	0.48	-	0.48	-
Core-valence	-1.32×10^{-2}	0.0	0.0	-	-1.12×10^{-3}	-	-1.70×10^{-3}	-
Tail	6.66×10^{-2}	0.23	0.23	-0.16	3.46	-0.73	3.46	-1.04
Total (Present)	35.04	31.60	31.88	1.157	189.29	-79.137	188.65	-112.18
Others [6]	35.01	31.598	31.598	1.163	188.6	-112.1	188.6	-112.1
Experiment [7]	35.02(4)	-	-	-	-	-	-	-

Ca$^+$	$\alpha^{(0)}(4S_{1/2})$	$\alpha^{(0)}(4P_{1/2})$	$\alpha^{(0)}(4P_{3/2})$	$\alpha^{(2)}(4P_{3/2})$	$\alpha^{(0)}(3D_{3/2})$	$\alpha^{(2)}(3D_{3/2})$	$\alpha^{(0)}(3D_{5/2})$	$\alpha^{(2)}(3D_{5/2})$
Main	72.80	-4.97	-2.96	10.74	26.23	-16.45	25.98	-23.11
Core	3.26	3.26	3.26	-	3.26	-	3.26	-
Core-valence	-8.85×10^{-2}	0.0	0.0	-	-7.94×10^{-3}	-	-1.20×10^{-2}	-
Tail	5.87×10^{-2}	2.52	2.52	-0.66	3.05	-0.62	2.84	-0.82
Total (Present)	76.03	0.82	2.82	10.08	32.31	-17.02	32.05	-23.92
Others [8]	75.28	-2.774	-0.931	10.12	32.99	-17.88	32.81	-25.16
Others [9]	76.1(5)	$-0.75(70)$	1.02(64)	10.31(28)	32.0(3)	$-17.43(23)$	31.8(3)	$-24.51(29)$
Experiment [10]	75.3(4)	-	-	-	-	-	-	

Sr$^+$	$\alpha^{(0)}(5S_{1/2})$	$\alpha^{(0)}(5P_{1/2})$	$\alpha^{(0)}(5P_{3/2})$	$\alpha^{(2)}(5P_{3/2})$	$\alpha^{(0)}(4D_{3/2})$	$\alpha^{(2)}(4D_{3/2})$	$\alpha^{(0)}(4D_{5/2})$	$\alpha^{(2)}(4D_{5/2})$
Main	85.73	-39.94	-28.44	11.33	53.83	-34.25	53.63	-46.33
Core	4.98	4.98	4.98	-	4.98	-	4.98	-
Core-valence	-0.19	0.0	0.0	-	-1.77×10^{-2}	-	-2.79×10^{-2}	-
Tail	1.97×10^{-2}	3.70	2.67	-0.81	4.95	-1.00	3.48	-1.01
Total(Present)	90.54	-31.27	-20.79	10.52	63.74	-35.26	62.08	-47.35
Other [11]	89.88	-23.13	-23.13	-	61.77	-	61.77	-
Other [12]	88.29(1.0)	-	-	-	61.43(52)	$-35.42(25)$	62.87(75)	$-48.83(30)$
Experiment [13]	93.3(9)	-32.6	-32.6	-	57.0	-	57.0	-

Ba$^+$	$\alpha^{(0)}(6S_{1/2})$	$\alpha^{(0)}(6P_{1/2})$	$\alpha^{(0)}(6P_{3/2})$	$\alpha^{(2)}(6P_{3/2})$	$\alpha^{(0)}(5D_{3/2})$	$\alpha^{(2)}(5D_{3/2})$	$\alpha^{(0)}(5D_{5/2})$	$\alpha^{(2)}(5D_{5/2})$
Main	114.19	6.85	32.00	5.87	39.71	-21.92	42.42	-30.37
Core	9.35	9.35	9.35	-	9.35	-	9.35	-
Core-valence	-0.38	0.0	0.0	-	-2.35×10^{-2}	-	-3.87×10^{-2}	-
Tail	1.66×10^{-2}	4.26	4.18	-1.17	4.76	-1.00	4.80	-1.47
Total (Present)	123.18	20.46	45.53	4.70	53.80	-22.92	56.53	-31.83
Other [12]	124.26(1.0)	-	-	-	48.81(46)	$-24.62(28)$	50.67(58)	$-30.85(31)$
Experiment [14]	123.88(5)	-	-	-	-	-	-	-

institute of standards and technology (NIST) database [5], we determine the "Main" contributions to valence correlations of α_ns of the $nS_{1/2}$, $nP_{1/2,3/2}$ and $mD_{3/2,5/2}$ states in the considered alkaline earth metal ions. In Table I, we list the contributions from the "Main", core, valence-core and "Tail" components to the static values of α_n for all the considered alkaline ions. The final values are compared with other available theoretical and experimental values. Transitions up to the $3S - 6P$, $3P - 6S$, $3P - 6d$, $3D - 6P$ and $3D - 7F$ are included into the "Main" contribution for Mg$^+$ ion. As seen from

Table I, the ground state dipole polarizability values obtained for the Mg$^+$ ion are very close to the values estimated by Mitroy and Zhang [6]. They evaluate the non-relativistic values of polarizabilities by diagonalizing the semi-empirical Hamiltonian in a large dimension single electron basis. We notice that there is a large difference between our polarizability results for $3D_{3/2}$ and $3D_{5/2}$ states and hence the non-relativistic values calculated by them are unfavorable. Snow [7] deduced the static polarizability for the ground state of the Mg$^+$ ion from the fine structure of high Rydberg levels. Their $\alpha^{(0)}$ value

of 35.02(0.04) a_0^3 agrees well with our result of 35.04 a_0^3. For Ca$^+$ ion transitions up to the $4S - 7P$, $4P - 7S$, $4P - 6d$, $3D - 7P$ and $3D - 7F$ are included into the "Main" contribution. While examining polarizabilities in case of the Ca$^+$ ion, we notice that our calculation for the ground state polarizability is in the agreement with the result obtained from experimental spectral analysis by Chang [10]. Also, a comparison of our calculated polarizabilities for this ion with the calculations done using combination of many-body perturbation theory and SD scaled method by Safronova *et al.* [9] shows very good agreement. Moreover, our result for the ground state is in consistent agreement with the results calculated by Tang and co-workers [8]. However, a discrepancy has been observed between our results and other calculations among the P state polarizabilities this ion. We notice that the polarizabilities of the P states are very small due to substantial cancellations between some large contributions to the total polarizability. The final values are, thus, very sensitive to these cancellations. Next, we compare our polarizability results for the Sr$^+$ ion in Table I. Transitions up to the $5S - 8P$, $5P - 8S$, $5P - 7d$, $4D - 8P$ and $3D - 7F$ are included into the "Main" contribution for this ion. Mitroy and coworkers [11] have used a non-relativistic method using a sum-over-states approach to determine polarizabilities of the S, P and D states of Sr$^+$.

It is evident from Table I that our ground state dipole polarizability is in agreement with their result. However, it may not be proper to compare their non-relativistic values of the polarizabilities for the $4D_{3/2}$ and $4D_{5/2}$ states just by including corrections from the relativistic effects with the non-relativistic values agnaist our fully relativistic calculations. However, the static dipole polarizabilities calculated for the ground and $4D$ state of the Sr$^+$ ion using an *ab initio* relativistic coupled-cluster method [12] are in close agreement with our results. There are no direct experimental values available to compare with these results. The polarizability values for the S, P and D states of the Sr$^+$ ion, derived by combining the experimental results with oscillator strength sums by Barklem and O'Mara [13], has a considerable discrepancy with our present results. In Ba$^+$ ion, transitions up to the $6S - 8P$, $6P - 8S$, $6P - 6d$, $5D - 8P$ and $5D - 7F$ are included into the "Main" contribution. The high-precision ground state polarizability measurement for Ba$^+$, achieved by using a novel technique, based on the resonant excitation Stark ionization spectroscopy [14], is in very good agreement with our work. To summarize, the above analysis clearly justifies that our calculations of dipole polarizabilities in the considered alkaline earth metal ions are accurate enough to predict the magic wavelengths in these ions reliably.

[1] J. Kaur, D. K. Nandy, B. Arora, and B. K. Sahoo, Phys. Rev A **91**, 012705 (2015).

[2] S. A. Blundell, W. R. Johnson, and J. Sapirstein, Phys. Rev A **43**, 3407 (1991).

[3] M. S. Safronova, A. Derevianko, and W. R. Johnson, Phys. Rev A **58**, 1016 (1998).

[4] M. S. Safronova, *Ph.D. Thesis* (University of Notre Dame, 2000).

[5] A. Kramida, Y. Ralchenko, J. Reader, and N. A. T. (2012), *Nist atomic spectra database* (2012), (version 5). [Online]. Available: http://physics.nist.gov/asd [2012, December 12]. National Institute of Standards and Technology, Gaithersburg, MD.

[6] J. Mitroy and J. Y. Zhang, Eur. Phys. J. D. **46**, 415 (2008).

[7] E. Snow, *Ph.D. Thesis* (Colorado State University, 2006).

[8] Y. B. Tang, H. X. Qaio, T. Y. Shi, and J. Mitroy, Phys. Rev. A **87**, 042517 (2013).

[9] M. S. Safronova and U. I. Safronova, Phys. Rev. A **83**, 012503 (2011).

[10] E. S. Chang, J. Phys. B: At. Mol. Phys. **16**, L539 (1983).

[11] J. Mitroy, J. Y. Zhang, and M. W. Bromley, Phys. Rev.A **77**, 032512 (2008).

[12] B. K. Sahoo, R. G. E. Timmermans, B. P. Das, and D. Mukherjee, Phys. Rev A **80**, 062506 (2009).

[13] P. S. Barklem and B. J. OMara, Mon. Not. R. Astron. Soc. **311**, 535 (2000).

[14] E. L. Snow and S. R. Lundeen, Phys. Rev. A **76**, 052505 (2007).